applied sciences

MDPI

Article

Pore Space Connectivity in Different Rock-Physics Methods—Similarity and Differences

Irina Berezina * and Irina Bayuk *

Schmidt Institute of Physics of the Earth of the Russian Academy of Sciences, 123242 Moscow, Russia
* Correspondence: iberezina@ifz.ru (I.B.); ibayuk@ifz.ru (I.B.)

Abstract: This study is focused on the analysis of pore space connectivity in reservoir rocks. This parameter is of vital importance for the oil and gas industry since it controls hydraulic permeability. Five methods of rock physics are used for this goal. Three of these methods (self-consistent version of generalized singular approximation, Berryman self-consistent method, and differential scheme) take into account the pore space connectivity implicitly. The other two methods, the f-model of the generalized singular approximation and a similar modification of the Berryman method suggested in this work, allow for quantifying the connectivity via a special parameter (f-parameter). In order to reveal a physical meaning of this parameter, two simple models of carbonate rock (porous-cracked limestone) are considered. The first model is a double porosity model containing spherical pores and cracks. The second model contains only spherical pores, and their connectivity is expressed via the f-parameter. The pores and cracks are filled with brine and gas. Application of the two groups of methods for modeling the effective elastic properties of the carbonate rock gives a possibility of relating the f-parameter to the characteristics of the cracks and pores. The f-parameter is shown to be controlled by the relative crack volume in the total pore space. An increase in crack porosity and crack density leads to an increase in the f-parameter. A good correlation of the f-parameter with crack density is demonstrated. It is shown that for the porosity range 2–20%, a relationship between the f-parameter and crack density ε, in general, has the form $f = a\log_{10}(\varepsilon)^2 + b\log_{10}(\varepsilon) + c$ for $\varepsilon \leq \varepsilon_{min}$. For the crack density less than ε_{min} the f-parameter can be approximated by a constant value f_{min}. The values of ε_{min} and f_{min} and coefficients a, b, and c depend on the porosity of spherical pores, saturation type, and pair of methods used for finding the link. These results give f-models an advantage in searching zones of the enhanced permeability and quantifying the ability of these zones to filtrate fluids.

Keywords: effective elastic properties; rock physics modeling; self-consistent method; connectivity; permeability

Citation: Berezina, I.; Bayuk, I. Pore Space Connectivity in Different Rock-Physics Methods—Similarity and Differences. *Appl. Sci.* **2022**, *12*, 10185. https://doi.org/10.3390/app121910185

Academic Editor: Arcady Dyskin

Received: 7 September 2022
Accepted: 7 October 2022
Published: 10 October 2022

1. Introduction

The permeability of sedimentary rocks is of great importance in controlling oil and gas production, hydrology, and the storage of carbon dioxide and radioactive waste in geologic formations. The hydraulic properties of porous rocks depend on the lithology, pressure, and pore network structure, which is controlled by pore sizes, length, aspect ratio, and connectivity [1,2]. The degree of connectivity between the pores highly affects the permeability of the rock [3–6]. Low-porosity rocks with well-connected voids may have a high permeability, in contrast with high-porosity rocks with poor-connected pore spaces such as micritic limestone or clays.

The notion of connectivity is very intuitive (the ability to be connective or connected); however, the qualitative definitions may vary depending on the area of research. In mathematics, we could specify the term "connectivity" or "connectedness" as a characteristic of topological space or as a term of graph theory where connectivity is defined by the number of ways that points are connected.

Imaging techniques such as X-ray microtomography allow us to visualize how pore space is arranged in a material. The quantitative analysis of these images gives detailed information about the basic textural properties, distribution, arrangement, and connectivity of the pores. For instance, Qian et al. [7] provided the investigation of shale pore structure characteristics by applying field emission or focused ion beam scanning electron microscopy (FE-/FIB-SEM). The integration of this microstructure data with other techniques is also beneficial for assessing the pore structure influence on flow properties. Combining computer tomography (CT) scanning and microscopic seepage simulation allowed authors to evaluate quantitatively the effectiveness of fractures [8]. Yang et al. [9] performed flow simulation on digital rock models obtained from CT data to investigate the effect of the adsorption boundary layer on the fluid flow. Jia and Xian [10] explored the permeability of shale by simulating pulse-decay experiments on a discrete fracture model based on 3D scanner results.

Arzilli et al. [11] proposed a methodology for estimating the pore connectivity in carbonate granular media using the number and size of the backbones (parts of the connected pore network) and the "cluster multiple labeling" techniques according to which connectivity is a ratio of the volume of the largest backbones of pores to the volume of all pores in the sample.

For carbonate grainstones, Zambrano et al. [12] provided an assessment of pore connectivity through the following parameters—connected porosity, specific surface, and connectivity density. Koestel et al. [13] considered connectivity measures such as the connection probability, the Euler density, and the critical pore diameter for soil samples.

Due to the limited resolution of the imaging technique and ambiguity in the identification of individual phases (segmentation problem) and in the definition of representative elementary volume, these quantitative characteristics may be difficult to identify in rocks containing microporosity, hence these connectivity measures are not reliable enough.

Owing to real porous space complexity for analyses of pore network morphologies, researchers usually apply some simplifications representing pore space as morphological (pore-throat) networks, consisting of spherical pores and cylindrical throats, or random networks. In this case, coordination number or mean coordination number and radius of the pore provide information about the pore connectivity [14–17]. The coordination number is the number of throats (channels) connected to a nodal pore, but connectivity metrics from percolation theory are also widely used. They are the percolation probability [18,19], the connected porosity [20], and the percolation threshold [19,21].

Glover [22] uses Archie's laws to propose a measure of connectivity. He defines connectedness as the inverse of the formation resistivity factor and shows that connectedness is the product of porosity and connectivity. The connectivity itself depends upon the porosity and the cementation exponent from Archie's law.

Montaron [23] associates the connectivity of a random network with the conductivity equations obtained from percolation and effective medium theory [24]. The author presents the connectivity equation with two parameters—a conductivity exponent and a water connectivity index. The combination of this equation with modified mixing law allows to account for variations of water connectivity within the rocks. Montaron [23] successfully applied his theory to obtain analytical conductivity models of shale sands, oil-wet rocks, and mixed-wet micritic carbonates.

Trinchero et al. [25] considered a groundwater flow through an aquifer and adopted the hydraulic response time between two points in a pumping test as a flow connectivity indicator.

Since permeability is a scale-dependent property, the main factor controlling the pore connectivity also should be considered to be dependent on the scale.

Effective medium methods are among the most powerful tools in the rock physics field. These methods allow to connect the rock microstructure parameters with its macroscopic physical properties. The design of a mathematical model of effective physical properties consists of three main steps: (1) construction of so-called "conceptual model"

that mimics specific features of the rock microstructure; (2) the parametrization of the model; (3) the choice of the rock-physics method, which relates the model parameters to the physical properties.

It is known that effective medium methods allow to predict the effective permeability for isotropic models via, for example, Bruggeman's approximation [26] proposed by Kirkpatrick [24,27] or anisotropic models via more advanced methods like the GSA [28,29] and T-matrix [30].

An example of application of effective medium theory (EMT) for the permeability estimation with the parameter f could be found in [31]. The authors applied the EMT (GSA method) for the effective permeability modeling for Barnett shale. They showed that for this modeling, the permeability of fluid-saturated zones should be dependent on the rock type and also specified (or inverted from the permeability measurements). Additionally, it was demonstrated that the f-parameter inverted from measured permeability has values similar to that inverted from the elastic wave velocities. In [32], the authors showed that the permeability of fluid-saturated zones depends on the fracture porosity to the power of 3.

In this work, we apply rock-physics methods to quantify pore/crack connectivity in porous-fractured limestone. Note that the term "crack" is commonly used in theory, but the term "fracture" is usually applied in practice. We quantified the pore connectivity in terms of a parameter (f-parameter) entered in some of the rock-physics methods. We consider this factor as a measure of pore/crack connection via the existence of cracks at a smaller scale level, which connect the pores at a larger scale. Cracks are specified by aspect ratio related to their aperture and volume concentration: crack porosity. The volume fraction of these cracks in rock is assumed to be small (less than 2%).

In practice, if we wish to obtain the connectivity (or crack parameters through the correlation with f-parameter) on the well-log scale, for example, we need some measurable property like elasticity (provided by sonic log). Then, solving the inverse problem for finding the parameters of the model, we will obtain the connectivity. Further, the fracture parameters could be inverted from the experimental data (for example, from elastic wave velocities, porosity, and density). The effective medium theory gives no possibility of taking into account the fracture length explicitly. The aspect ratio of fractures could be seen as the ratio of height to length of the fracture or as fracture aperture. If we consider the double porosity model, then we could evaluate the aspect ratio of fractures and their volume fraction. If we consider the f-model and the pores as "round" fractures, then we could evaluate their connectivity, aspect ratio, and volume fraction. In our work, we do not consider the inversion of the fracture parameters since we have another goal. Note that in all EMT methods, the void's size is not taken into account explicitly. Thus, the volume fraction of inclusions can be increased by the increasing the void's number but keeping their shape and size or by increasing the void's length and/or opening and keeping the void's number. In the case of elasticity, the EMT formulas give the same results for these two types of increasing the volume fraction of voids. However, when dealing with the effective permeability, as was shown by our previous modeling, the void's size should be implicitly incorporated in the permeability of so-called fluid-conductive zones [31,32]. This parameter is included in the list of unknowns and inverted from experimentally measured permeability.

We consider two types of conceptual models (Type 1 and Type 2) of porous-cracked limestone. They include the mineral grains, pores, and fractures whose shape is approximated by ellipsoids having various aspect ratios. The classification depends on a way how the void's connectivity is represented. The Type 1 model is the double porosity model. In this model, the pores are connected via randomly oriented cracks. The void's connectivity in the Type 1 model is taken into account implicitly. The Type 2 model assumes that a rock contains only pores and the pore connectivity is explicitly described by the f-parameter, which is an empirical factor expressing a degree of void's connectivity. These models are applicable for isotropic formations without subvertical cracks at the core and

well-log scales. Note that the model complexity highly dependents on the problem, thus the construction of the model is a balance between the oversimplification and preserving the geological realism.

For calculating the effective elastic properties, we apply five methods of effective medium theory. Each of the methods is applicable for the model of Type 1 or Type 2.

Matching the calculated effective elastic properties between two selected models (one model of Type 1 and the other model of Type 2) we obtain a relation between values of f-parameter and a pair of parameters characterizing the crack morphology—crack aspect ratio and porosity. Moreover, we find similar relations between the f-parameter and crack density and specify them in the form of equations.

2. Materials and Methods

2.1. Basic Principles of Effective Medium Theory

We assume that rock is a micro-inhomogeneous material that can be in general macroscopically anisotropic. Macroscopic properties (or effective properties) of this material averaged over a representative volume (REV) are controlled by the properties of mineral grains and materials filling pores and cracks (inclusions), and also by inclusion's shape, orientation, and spatial distribution. REV should be a statistically homogeneous media. In addition, REV should be large enough compared to the characteristic size of heterogeneities and, on the contrary, REV should be small enough compared to the fluctuation length of macroscopic fields (specifically, wavelength). Thereafter the EMT methods provide a determination of the physical properties (elastic and transport) of heterogeneous media.

In the case of elasticity, the macroscopic properties of a heterogeneous medium are described by the effective stiffness tensor $\mathbf{C}^*$ that relates, via the Hook law, the strain ε and stress σ fields averaged over the REV. The problem of determination of effective properties leads to a multiparticle problem that can be solved only approximately. Consequently, for random media only approximation methods exist. The majority of EMT methods are based on the Eshelby problem solution for the strain filed in ellipsoidal inclusions placed in the infinite matrix [33]. Thereafter, all heterogeneities have the shape of general ellipsoids that can be characterized by two aspect ratios. For simplicity, ellipsoids of revolution are used whose shape can be specified by a single aspect ratio α. Among a variety of EMT methods we choose the following ones: the self-consistent method of Berryman [34], differential effective medium (DEM) [35], and two versions (self-consistent and f-model) of generalized singular approximation (GSA) [28,29]. Besides, we suggest our own version of Berryman's method to parametrize the void's connectivity via the f-parameter.

Our choice is motivated by the method's ability to take into account the connection of inclusion implicitly or explicitly.

2.2. Models of Fractured Carbonate Rock

The two models of porous-cracked limestone considered to find a correlation between connectivity factor f and crack's characteristics are shown in Figure 1. The first one (Type 1 model) is a double porosity model (Figure 1a). It consists of an isotropic matrix and two types of voids—pores and randomly oriented cracks saturated with a fluid. Crack aspect ratio α_{crack} varies from 10^{-5} to 0.1, and crack volume fraction (crack porosity) ϕ_{crack} does not exceed 2%. Pore aspect ratio α_{pore} is equal to 1. The aspect ratio of calcite grains is also equal to 1.

The second model (Type 2 model) is a so-called f-model (Figure 1b) [29,36], which takes into account the connectivity of the voids via a special parameter f. In contrast to the double porosity model here only spherical saturated pores are embedded in the matrix. An empirical factor f reflects the connectivity of the pores and varies from 0 to 1. Pore volume fraction ϕ_{pore} changes from 0 to 20% for both models.

Considering the carbonate rock model, we use the calcite matrix (isotropic polycrystal) with brine- and gas-filled voids. The bulk and shear moduli of the matrix are equal to 72.0

and 32.0 GPa respectively. The brine bulk modulus is 2.5 GPa, and the gas bulk modulus is 0.006 GPa. The shear modulus of fluids is zero.

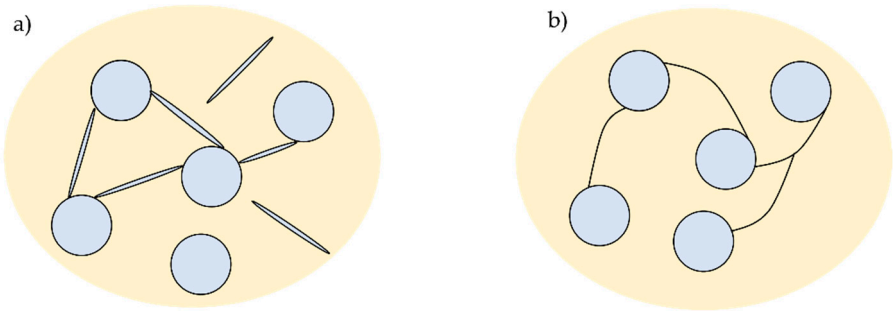

Figure 1. The illustration of proposed models of porous-cracked limestone: (**a**) double porosity model (Type 1 model), (**b**) f-model (Type 2 model).

2.3. Generalized Singular Approximation Method (GSA)

The general formula for effective stiffness tensor $\mathbf{C}^*$ evaluation in the GSA method is [28,29,36]:

$$\mathbf{C}^* = \left\langle \mathbf{C}(\mathbf{r})\left[\mathbf{I} - \mathbf{g}\mathbf{C}'(\mathbf{r})\right]^{-1}\right\rangle \left\langle \left[\mathbf{I} - \mathbf{g}\mathbf{C}'(\mathbf{r})\right]^{-1}\right\rangle^{-1}, \quad (1)$$

where angle brackets mean averaging over the representative volume; $\mathbf{C}(\mathbf{r})$ is the fourth-rank tensor of the elastic constants related to the calcite matrix or fluid filling the voids; $\mathbf{I}$ is the unit fourth-rank tensor; $\mathbf{g}$ is the Green function tensor, defined by the equation:

$$g_{ijkl} = -\frac{1}{16\pi}\int_0^{2\pi}\int_0^{\pi}\left(n_{kj}\Lambda_{il}^{-1} + n_{ki}\Lambda_{jl}^{-1} + n_{lj}\Lambda_{ik}^{-1} + n_{li}\Lambda_{jk}^{-1}\right)\sin\theta \mathrm{d}\theta \mathrm{d}\varphi, \quad (2)$$

where $\theta \in [0,\pi]$, $\varphi \in [0,2\pi)$ and $\Lambda_{ij} = C^c_{ijkl}n_k n_l$, $i,j,k,l = 1,2,3$ with $n_1 = \sin\theta\cos\varphi/a_1$, $n_2 = \sin\theta\sin\varphi/a_2$, $n_3 = \cos\theta/a_3$; a_1, a_2, a_3 are semi-axes of the ellipsoidal inclusions. The tensor $\mathbf{C}'(\mathbf{r}) \equiv \mathbf{C}(\mathbf{r}) - \mathbf{C}^c$ is the fluctuation of the stiffness tensor. The tensor $\mathbf{C}^c$ is the elastic tensor of the comparison body whose parameters could be arbitrary [28]. All indices in Equation (2) vary from 1 to 3.

If we set $\mathbf{C}^c$ equal to the stiffness tensor of the medium with the effective properties $\mathbf{C}^c = \mathbf{C}^*$, then it gives us the formulas of the self-consistent method (GSA-SC) [28,37].

This equation represents one of several realizations of self-consistent methods. The main idea of this approach is based on two hypotheses: (1) every inclusion acts like an isolated one in the medium with the effective properties of the composite and (2) the field acting on every inclusion is the external field applied to the medium. Thus, both hypotheses reduce the problem of interaction between many inclusions to a one-particle problem. In general, the self-consistent method gives good predictions for polycrystals and is a bit less accurate in the case of matrix composites.

If we consider porous space connectivity in the f-model, we express the comparison body properties as a linear combination of the matrix and fluid properties according to Equation (3) [29]:

$$\mathbf{C}^c = (1-f)\mathbf{C}^M + f\mathbf{C}^{fl}, \quad (3)$$

where $\mathbf{C}^M$ and $\mathbf{C}^{fl}$ are, respectively, the stiffness tensors of the mineral matrix (the stiffest component) and fluid filling the voids (the softest component); f is an empirical dimensionless parameter reflecting connectivity of the voids.

Jiang [38] shows that, in the general case, the parameter f is a tensor and the following expressions are valid:

$$\mathbf{f} = \alpha\boldsymbol{\varepsilon}^{fl}\left(\boldsymbol{\varepsilon}^C\right)^{-1}, \mathbf{I} - \mathbf{f} = \alpha\boldsymbol{\varepsilon}^M\left(\boldsymbol{\varepsilon}^C\right)^{-1}, \quad (4)$$

where $\mathbf{f}$ is a "connectivity tensor"; α is the poroelastic Biot-Willis parameter [39–41]; $\boldsymbol{\varepsilon}^{fl}$, $\boldsymbol{\varepsilon}^M$ and $\boldsymbol{\varepsilon}^C$, are, respectively, the strain fields in the fluid inclusions, matrix, and com-

parison body. Thus, the physical meaning of the f-parameter specifies the deformation field distribution in the medium when the heterogeneous body reaches an equilibrium state.

If f = 1 in Equation (4), we get the lower Hashin-Shtrikman bound ($\mathbf{C}^{c} = \mathbf{C}^{fl}$). In this case, we have an artificial medium where the pore space is connected and ellipsoidal particles of mineral material are enveloped by fluid with no direct contact between them. In such a case, the deformation of the fluid inclusion will make the largest contribution to the overall deformation and $\boldsymbol{\varepsilon}^{C} = \boldsymbol{\varepsilon}^{fl}$. Furthermore, this situation is a representation of an unconsolidated medium, which Biot–Willis parameter $\alpha \approx 1$ [42]. In the opposite case when f = 0, we get the upper Hashin–Shtrikman bound, all voids become isolated and the matrix is a connected space. Therefore, the deformation of the matrix will contribute the most to the overall deformation and $\boldsymbol{\varepsilon}^{C} = \boldsymbol{\varepsilon}^{M}$. Note that all real cases met in practice correspond to parameter f between 0 and 1. A sensitivity study of effective stiffness tensor to parameter f exhibits a non-linear behavior. The elastic moduli become to decay faster as f approaches 1. A relation of parameter f with permeability is also analyzed in [43] where the authors demonstrated that this parameter is proportional to $\ln(k/\phi)$, where k is the permeability and ϕ is the porosity.

In our models described in the previous section, the particles of mineral matrix, pores and cracks are considered the inclusions. For Type 1 model, N = 3 and the volume concentration of mineral matrix is $v_1 = 1 - (v_2 + v_3)$ where $v_2 = \phi_{pore}$ and $v_3 = \phi_{crack}$ are the volume concentrations of pores and crack, respectively. For Type 2 model, N = 2 and $v_1 = 1 - v_2$ where $v_2 = \phi_{pore}$. The pieces of mineral matrix are considered to be spherical.

We can rewrite Equation (1) in the form:

$$\mathbf{C}^{*} = \left(\sum_{i} v_i \mathbf{C_i} \int \mathrm{P_i}(\theta, \varphi, \psi)[\mathbf{I} - \mathbf{g}_i(\mathbf{C}_i - \mathbf{C^c})]^{-1} \sin\theta \mathrm{d}\theta \mathrm{d}\varphi \mathrm{d}\psi \right) \times \left(\sum_{i} v_i \int P_i(\theta, \varphi, \psi)[\mathrm{I} - \mathbf{g}_i(\mathbf{C}_i - \mathbf{C^c})]^{-1} \sin\theta \mathrm{d}\theta \mathrm{d}\varphi \mathrm{d}\psi \right)^{-1} \quad (5)$$

where $\mathbf{g}_i$ is the Green function tensor of the inclusions of type i defined by the Equation (2). The tensor $\mathbf{C}_i$ is the stiffness tensor of i-th type of inclusions. The function P_i is the probability density function of distribution of the inclusions over their orientations; θ, φ, ψ are the Eulerian angles describing the inclusion orientation in space. The tensors $\mathbf{I}$ and $\mathbf{C}^{c}$ have the same meaning as in Equations (1) and (2).

2.4. Berryman's Method

Berryman's method [34] is another realization of the self-consistent effective medium methods [44–47]. Based on the results of Kuster and Toksoz [48], Berryman obtained expressions for calculating the effective moduli (Equation (6)) of an isotropic matrix with randomly oriented ellipsoidal isotropic inclusions. Note that in this method no host medium is assumed. The pieces of mineral material, pores, cracks, and other impurities are considered as ellipsoidal inclusions. The formulas for calculating the effective elastic moduli have the form:

$$\sum_{i=1}^{N} \nu_i (K_i - K^{*}_{SC}) P^{*i} = 0, \ \sum_{i=1}^{N} \nu_i (\mu_i - \mu^{*}_{SC}) Q^{*i} = 0, \quad (6)$$

where K^{*}_{SC} and μ^{*}_{SC} are effective bulk and shear moduli; K_i and μ_i are the inclusion's bulk and shear moduli, ν_i are the volume fractions of inclusions, N is the number of inclusion types. The coefficients P^{*i} and Q^{*i} depend on the inclusion's shape and properties of the effective medium. Equations of the P^{*i} and Q^{*i} for the general case of ellipsoidal inclusions are rather bulky and are not shown here. They can be found in [48]. Equation (6) contain unknown effective elastic moduli in the both left- and right-hand sides. Such equations are solved by iterations.

Note that Equation (6) can be written in a form more convenient for computations:

$$K^*_{SC\text{-}f} = \sum_{i=1}^{N} \nu_i K_i P^{*i} / \sum_{i=1}^{N} \nu_i P^{*i},\ \mu^*_{SC\text{-}f} = \sum_{i=1}^{N} \nu_i \mu_i Q^{*i} / \sum_{i=1}^{N} \nu_i Q^{*i}, \quad (7)$$

Equations (6) and (7) are the results of a series of long-wavelength scatterings experiments. During the experiments, a small sphere of the true composite material (heterogeneous material) is embedded in a medium whose properties are changed in a controlled manner, achieving zero scattering from the composite sphere. If we change the sphere properties to comparison body properties and consider comparison body properties as provided by Equation (3) with f-parameter, we derive an alternative version of Berryman's formulas accounting for pore connectivity. Note that in this case there is no need for an iteration scheme as for Equation (6) or (7).

$$K^*_{SC\text{-}f} = \sum_{i=1}^{N} \nu_i K_i P^{Ci} / \sum_{i=1}^{N} \nu_i P^{Ci},\ \mu^*_{SC\text{-}f} = \sum_{i=1}^{N} \nu_i \mu_i Q^{Ci} / \sum_{i=1}^{N} \nu_i Q^{Ci}, \quad (8)$$

where P^{Ci} and Q^{Ci} are evaluated similarly to those as in Equations (6) and $K^* = K^C$, $\mu^* = \mu^C$. The comparison body moduli K^C and μ^C are found by analogy with Equation (3):

$$K^C = (1-f)K^M + fK^{fl},\ \mu^C = (1-f)\mu^M + f\mu^{fl}, \quad (9)$$

where K^M, μ^M are the bulk and shear moduli of the mineral matrix (the stiffest component); K^{fl}, μ^{fl} are the bulk and shear moduli of the fluid filling the voids (the softest component); f is an empirical parameter, reflecting connectivity of the saturated voids.

As in the previous section, for our modeling $N = 3$ for Type 1 model and $N = 2$ for Type 2 model. Inclusions are pieces of mineral matrix, pores, and cracks in Type 1 model. For Type 2 model the inclusions are pieces of mineral matrix and pores. The pieces of mineral matrix are assumed to be spherical.

2.5. Differential Effective Medium (DEM) Method

Differential effective medium theory [26,35,49–51] represents an iterative approach for calculating the effective elastic properties. This approach consists of the sequential introduction of the entire volume of inclusions in infinitesimal portions. At each step, the problem of finding the effective elastic properties of a material consisting of a matrix and inclusions is solved with the use of equations similar to (7) with the comparison body moduli equal to the effective moduli calculated at the previous step. As a result, a nonlinear differential equation or a system of such equations of the first order is obtained for calculating the effective elastic moduli of the medium (Equation (10)). As an initial step, we can assume the equality of the elastic moduli of the effective medium to the elastic moduli of the mineral matrix. The equations have the form:

$$(1-\nu)\frac{\partial K^*_{\mathrm{DEM}}}{\partial \nu} = (K_i - K^*_{DEM}(\nu))P^{*i},\ (1-\nu)\frac{\partial \mu^*_{\mathrm{DEM}}}{\partial \nu} = (\mu_i - \mu^*_{\mathrm{DEM}}(\nu))Q^{*i}, \quad (10)$$

where K^*_{DEM} and μ^*_{DEM} are the effective bulk and shear moduli; K_i and μ_i are the inclusion's bulk and shear moduli; ν is the volume fraction of inclusion which equals porosity here; P^{*i} and Q^{*i} depend on the shape of the inclusions and properties of the host (effective) medium.

In our modeling with DEM, we apply the iteration method for solving the differential Equation (10). At each iteration, first, we insert a small portion of cracks and, then, we add a small portion of pores. The iterations are carried our until we reach given values of ϕ_{pore} and ϕ_{crack}.

One practical detail of the application of the DEM is that the final result for a medium with several kinds of inclusions would depend on embedding the order of different components into the matrix.

3. Results

By comparing the effective elastic properties obtained for two types of carbonate rock, we can associate the f-parameter values with the crack's aspect ratio and porosity.

For the estimation of effective elastic moduli of the double porosity model we apply the classical self-consistent method of the effective medium theory (GSA-SC), Berryman's method (Berryman-SC), and DEM. In the case of GSA-SC and Berryman-SC, the pores, cracks, and calcite grains are embedded in effective media simultaneously, while in the case of the DEM, we insert the saturated voids in the calcite matrix sequentially: cracks at first and then the spherical pores.

Regarding the calculation procedure for the self-consistent methods (GSA-SC and Berryman-SC), we use an iterative scheme, in which properties of effective media were obtained in the previous iteration step. In the initial step, we take the elastic characteristics of effective media calculated with the Hill approximation (average of the results provided by Voigt and Reuss methods). The iterative procedure is stopped if the maximum change of moduli is less than 0.01 GPa.

We vary the aspect ratio of cracks α_{crack} from 10^{-4} to 0.1, and crack porosity ϕ_{crack} from 0 to 2%, and we calculate the effective properties for all possible combinations of these parameters. Instead of α_{crack} and ϕ_{crack}, we use the decimal logarithm of these parameters as it is more convenient for calculation and visualization. For obtaining f-model properties we use the generalized singular approximation method (GSA-f) and modification of the Berryman method (Berryman-f) with the introduced parameters f that is changing from 0 to 1. All these calculations are performed for different but fixed porosity of spherical pores ϕ_{pore} varying from 2 to 20%.

Then, we choose the pairs of moduli (bulk and shear) from the double porosity model (Type 1) and f-model (Type 2) whose difference is less than 0.1 GPa. This value of the threshold is chosen since, commonly, in geophysics, the bulk and shear moduli of minerals and rocks are specified with one decimal place.

Figures 2 and 3 show scatter plots resulting in pairs of $\log_{10}(\alpha_{crack})$ and $\log_{10}(\phi_{crack})$ versus f-parameter colored depending on the values of f-parameter. The volume fraction of spherical pores is fixed for each realization. We consider the cases when the spherical porosity equals 2, 5, 15, and 20%. Besides we analyze the behavior of the f-parameter vs. crack density for fixed spherical porosity (Figure 4). The crack density is a convenient parameter combining the crack porosity and aspect ratio thereby providing a single parameter to characterize fractured zones. The formula for the crack density has the form

$$\varepsilon = \frac{3\phi crack}{4\pi\alpha crack}. \tag{11}$$

In Figures 2 and 3 we observe some tendencies common for three pairs of methods: (1) GSA-SC − GSA-f, (2) Berryman-SC − Berryman-f, and (3) DEM − Berryman-f. As follows from Figures 2 and 3 the values of the f-parameter reflecting pore connectivity increase with increasing crack porosity for a fixed aspect ratio. Assuming brine saturated voids (Figure 2), for low porosities (less than 10%) the presence of a high volume of cracks increases the f-parameter more significantly than for higher porosities.

As seen in Figure 2, the maximum values of the f-parameter depend on the spherical porosity of brine-filled pores. Thus, the f-parameter reaches a maximum of 0.7 (Berryman-SC − Berryman-f) and 0.6 (DEM − Berryman-f) for 20% volume fractions of spherical pores. However, for low porosity (2%) these values are higher attaining, respectively, 0.98 and 0.97. As follows from Figure 2 the possible maximum value of f-parameter tends to decrease with increasing porosity and it is true for all pairs of methods. The results shown in Figure 2 suggest that this is more pronounced for sufficiently open cracks (aspect ratio is greater than 10^{-3}). The reason for a decrease in the f-parameter with spherical porosity (for constant crack porosity) is that the relative volume of cracks in the total porosity (the ratio of the crack porosity to the total porosity) decreases. This result is in line with the proportionality of the f-parameter to the permeability-to-porosity ratio reported in the work [34] since the permeability is greatly affected by connected cracks.

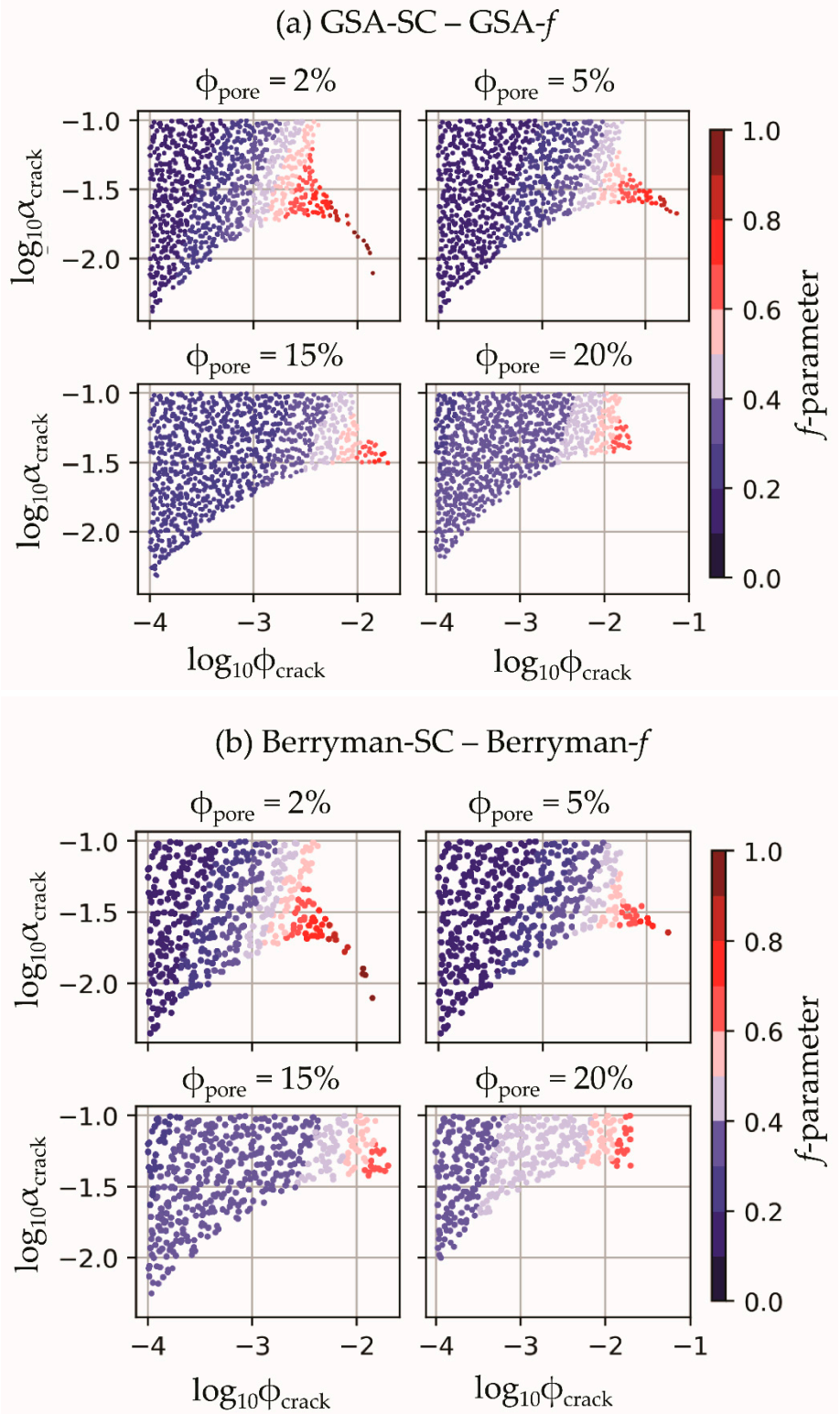

Figure 2. *Cont.*

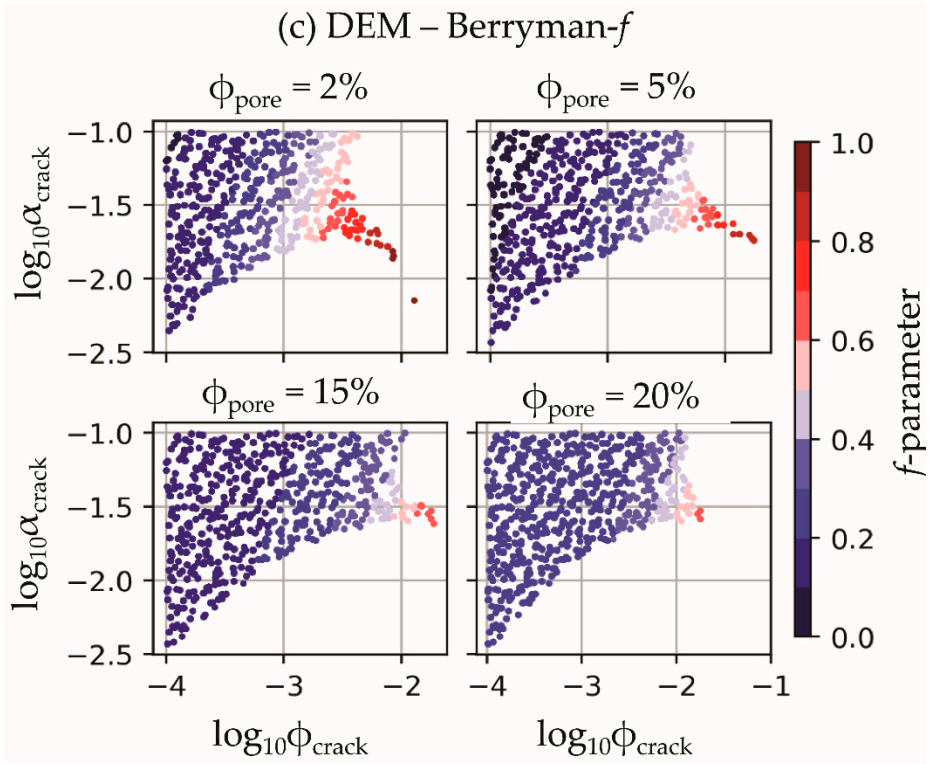

Figure 2. Crack aspect ratio and crack porosity vs. f-parameter as a color for fixed spherical porosity values. Voids are brine saturated. Calculations are performed for three pairs of methods: (**a**) GSA-SC—GSA-f, (**b**) Berryman-SC—Berryman-f, and (**c**) DEM—Berryman-f. Each color point is related to a solution for aspect ratio and crack porosity provided by Type 1 model. The color is controlled by the f-parameter value provided by Type 2 model.

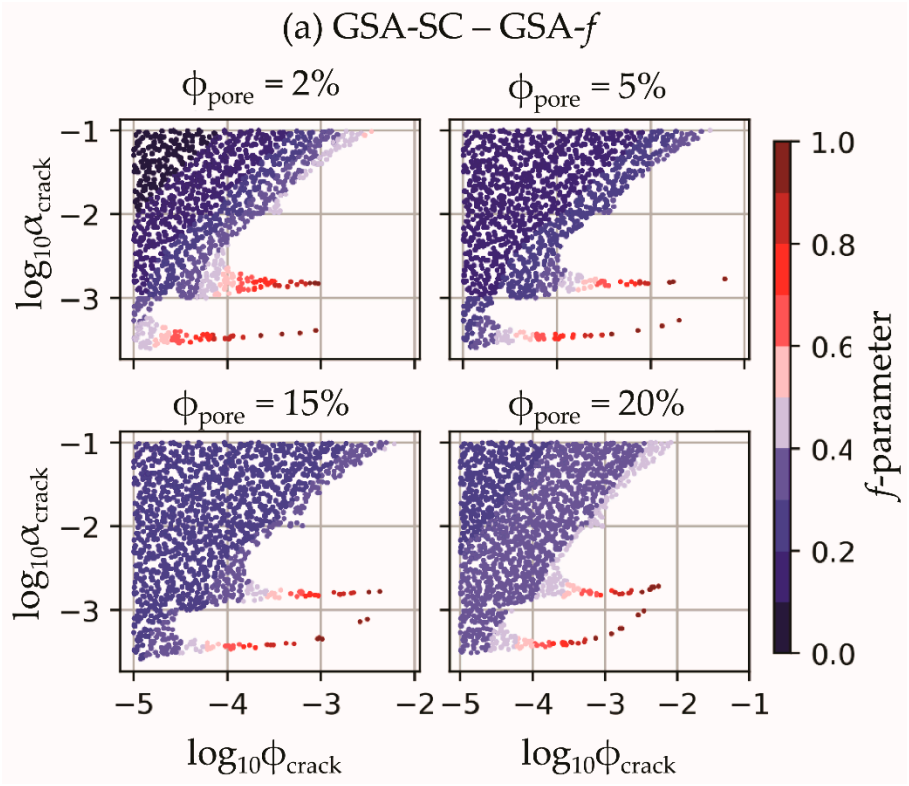

Figure 3. *Cont.*

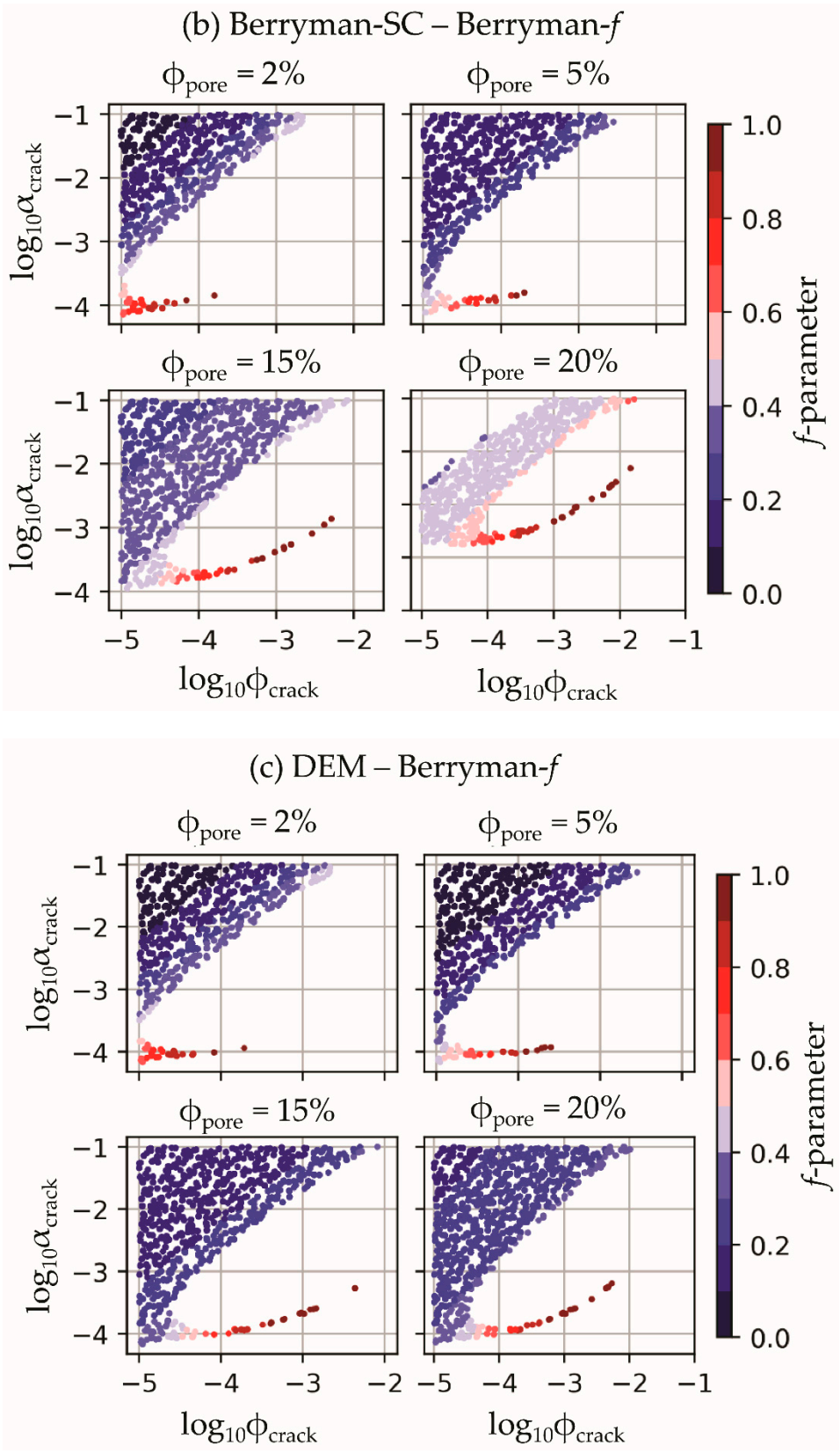

Figure 3. Crack aspect ratio and crack porosity vs. f-parameter as a color for fixed spherical porosity values. Voids are saturated with gas. Calculations are performed for three pairs of methods: (**a**) GSA-SC − GSA-f, (**b**) Berryman-SC − Berryman-f, and (**c**) DEM − Berryman-f. Each color point is related to a solution for aspect ratio and crack porosity provided by Type 1 model. The color is controlled by the f-parameter value provided by Type 2 model.

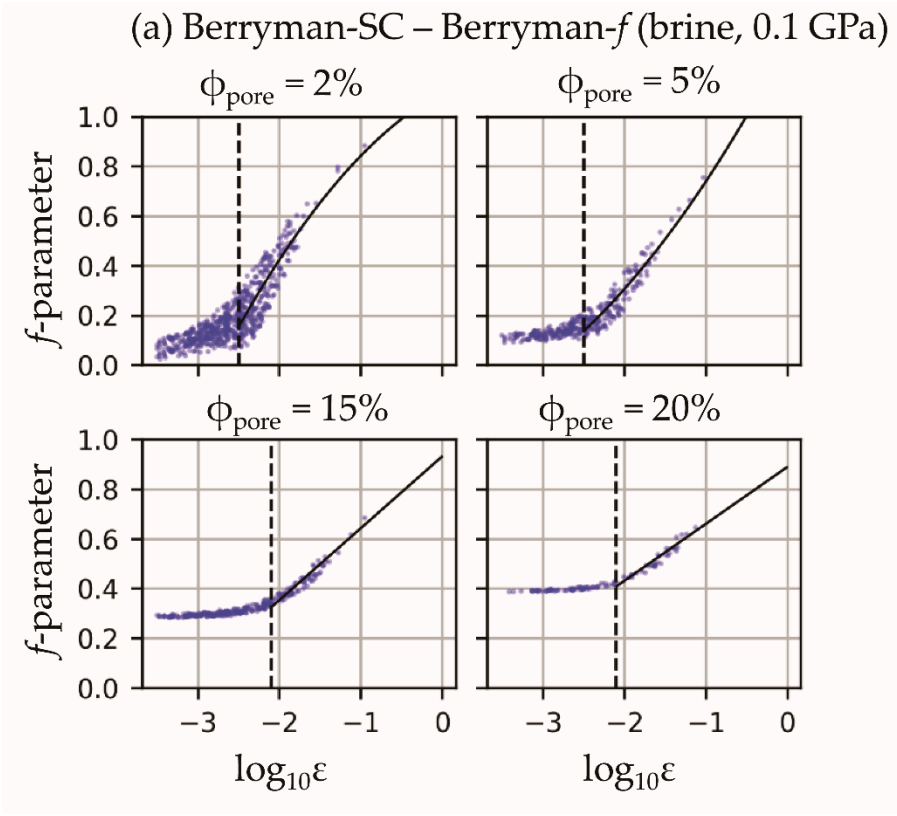

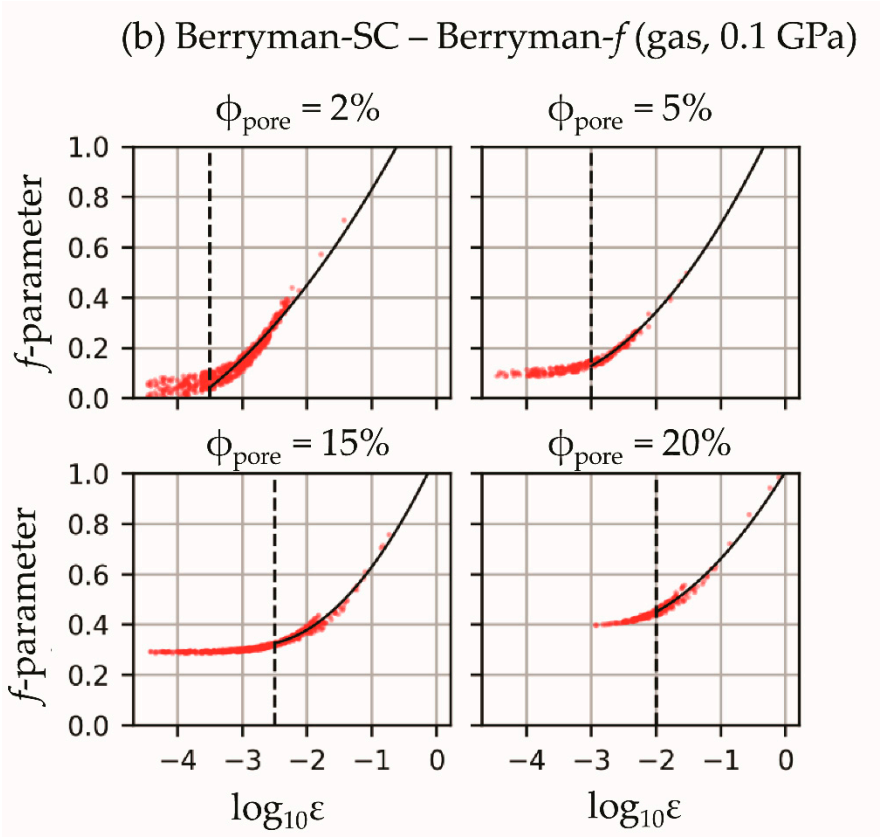

Figure 4. *Cont.*

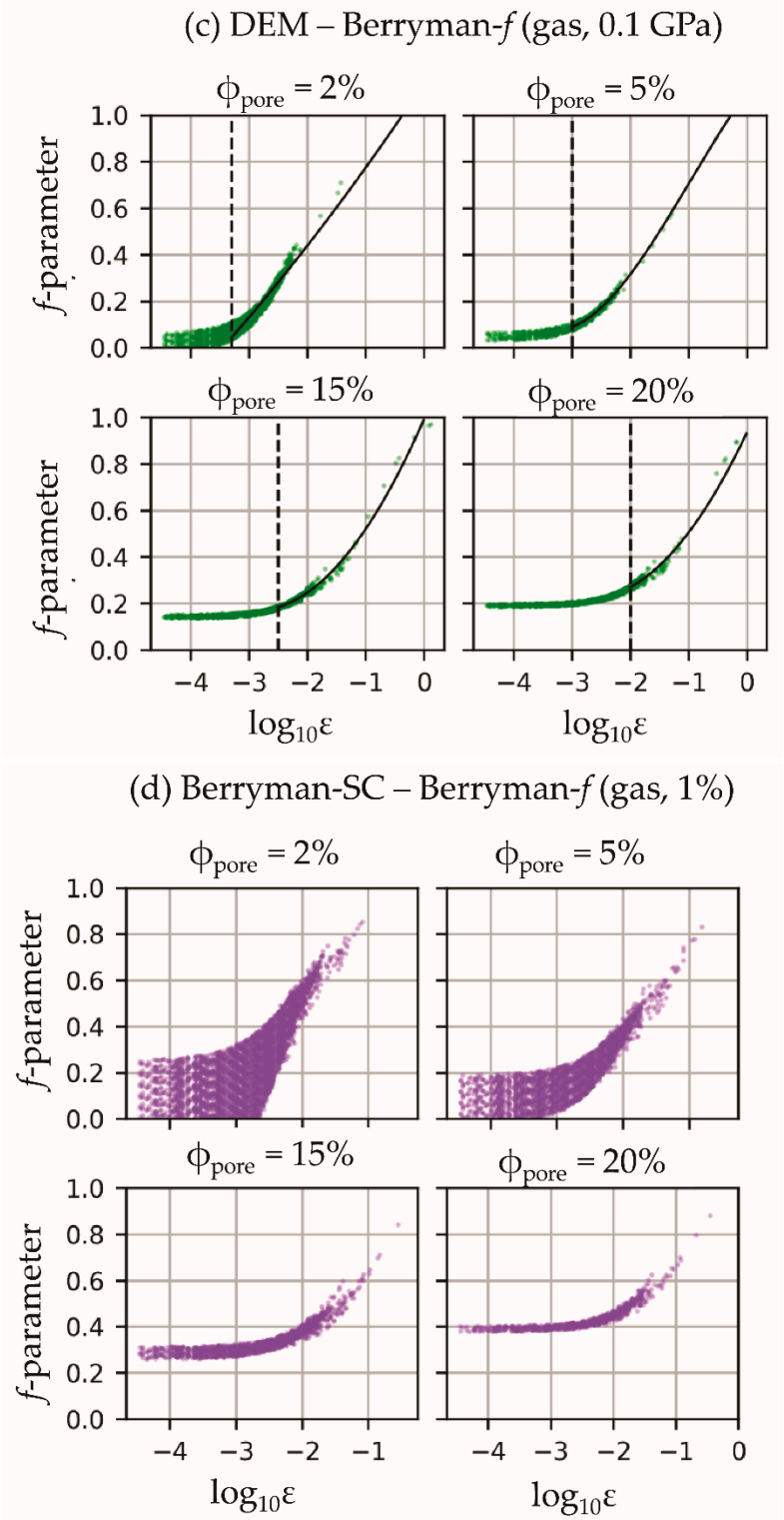

Figure 4. The *f*-parameter vs. crack density for fixed spherical porosity values. Effective properties are calculated with Berryman's methods, voids are (**a**) brine and (**b**) gas saturated; (**c**) with DEM and Berryman-*f* methods, voids are gas saturated. The accepted difference between the effective moduli provided by Type 1 and Type 2 models in cases (**a**–**c**) is chosen as 0.1 GPa. (**d**) Effective properties are calculated with Berryman's methods, voids are gas-saturated; the accepted difference between the effective moduli provided by Type 1 and Type 2 models is chosen as 1%. The meaning of numbers in parentheses is (type of saturation, accepted difference between the effective moduli provided by Type 1 and Type 2 models).

In Figure 2, a slight increase in the f-parameter is observed as the crack aspect ratio (or crack relative opening) decreases at the fixed crack porosity. This means that for fixed crack length, more cracks of lower aspect ratio should exist in rock to keep the same crack porosity as for more open cracks. In turn, the increase in crack number enhances the probability of cracks being connected. Thus, this result seems to be logical.

Similar dependences for gas-saturated voids are shown in Figure 3. Again, we see a tendency for an increase in the f-parameter with crack porosity. However, now solutions for very thin cracks (aspect ratio around 10^{-4}) can be obtained. For these thin cracks, we observe another behavior of the f-parameter with porosity. Namely, we can see the high values of connectivity parameter in the whole range of spherical porosity without a tendency to decrease with porosity. As the cracks become more open the effect of a decrease in this parameter with the spherical porosity (as is observed for brine-saturated pores) starts to manifest itself.

If we compare the results of three pairs of methods, we notice that the results of the first two pairs GSA-SC − GSA-f, and Berryman-SC − Berryman-f are almost identical for brine-saturated voids. It follows from that GSA and Berryman methods give the same effective moduli for spherical inclusions. In the case of gas-saturated voids, i.e., the media with a greater difference in elastic properties between matrix and fluids, the results on the scatter plots are slightly different (Figure 3).

Figure 4 demonstrates the dependence of the f-parameter on the decimal logarithm of crack density. Figure 4a,b shows the results for pairs Berryman-SC − Berryman-f for brine and gas-saturated models, respectively. Figure 4c exemplifies similar dependences for pair DEM − Berryman-f for gas-saturated case. The chosen measure of closeness in the elastic moduli for all of these cases is 0.1 GPa. A pronounced positive correlation of the f-parameter with the crack density is observed. For comparison we also show the results for pair Berryman-SC − Berryman-f for gas-saturated model but for another measure of closeness in the elastic moduli obtained by the two methods, namely, 1% (Figure 4d). As seen, in this case, the results are more scatter compared to the same model but for measure of closeness 0.1 GPa.

Regarding the relationship between the f-parameter and crack density, Figure 4 show that for fixed spherical porosity, the connectivity factor equals certain constant value until the crack density reaches its critical value (mark with dashed black line). After this point, the connectivity begins to increase steadily. We represent this behavior as the piecewise continuous function (Tables 1 and 2). For the most curves the increasing part is approximated with the following function $f = a \log_{10}(\varepsilon)^2 + b \log_{10}(\varepsilon) + c$. The obtained coefficients a, b, and c (Tables 1 and 2) in the equations for the pairs GSA-SC − GSA-f, and Berryman-SC − Berryman-f are quite close. Interesting, that the constant f-value for the Berryman-SC − Berryman-f and GSA methods are increasing together with the spherical porosity. Thus, higher porosities demonstrate higher connectivity even with the small crack densities. The DEM– Berryman-f results show noticeably lower connectivity values (Figure 4c) for a wider range of the crack's aspect ratios and porosities than the pairs GSA-SC − GSA-f and Berryman-SC − Berryman-f.

Table 1. Relationships between the crack density and f-parameter for fixed spherical porosity values for the case of brine-saturated voids. The R^2 is the coefficient of determination.

$\varphi_{\mathbf{pore}}$, %	Equation	$\mathbf{R^2}$
Berryman-SC − Berryman-f and GSA-SC − GSA-f		
2	$f = \begin{cases} -0.08\log_{10}(\varepsilon)^2 + 0.17\log_{10}(\varepsilon) + 1.10, & \log_{10}(\varepsilon) \geq -2.5 \\ 0.15, & \log_{10}(\varepsilon) < -2.5 \end{cases}$	0.74
5	$f = \begin{cases} 0.06\log_{10}(\varepsilon)^2 + 0.62\log_{10}(\varepsilon) + 1.30, & \log_{10}(\varepsilon) \geq -2.5 \\ 0.19, & \log_{10}(\varepsilon) < -2.5 \end{cases}$	0.88
10	$f = \begin{cases} 0.13\log_{10}(\varepsilon)^2 + 0.77\log_{10}(\varepsilon) + 1.34, & \log_{10}(\varepsilon) \geq -2.2 \\ 0.25, & \log_{10}(\varepsilon) < -2.2 \end{cases}$	0.93
15	$f = \begin{cases} 0.29\log_{10}(\varepsilon) + 0.93, & \log_{10}(\varepsilon) \geq -2.1 \\ 0.34, & \log_{10}(\varepsilon) < -2.1 \end{cases}$	0.95
20	$f = \begin{cases} 0.23\log_{10}(\varepsilon) + 0.89, & \log_{10}(\varepsilon) \geq -2.1 \\ 0.45, & \log_{10}(\varepsilon) < -2.1 \end{cases}$	0.95
DEM − Berryman-f		
2	$f = \begin{cases} -0.08\log_{10}(\varepsilon)^2 + 0.19\log_{10}(\varepsilon) + 1.10, & \log_{10}(\varepsilon) \geq -2.5 \\ 0.19, & \log_{10}(\varepsilon) < -2.5 \end{cases}$	0.71
5	$f = \begin{cases} 0.05\log_{10}(\varepsilon)^2 + 0.56\log_{10}(\varepsilon) + 1.20, & \log_{10}(\varepsilon) \geq -2.5 \\ 0.15, & \log_{10}(\varepsilon) < -2.5 \end{cases}$	0.85
10	$f = \begin{cases} 0.15\log_{10}(\varepsilon)^2 + 0.86\log_{10}(\varepsilon) + 1.34, & \log_{10}(\varepsilon) \geq -2.2 \\ 0.17, & \log_{10}(\varepsilon) < -2.2 \end{cases}$	0.92
15	$f = \begin{cases} 0.15\log_{10}(\varepsilon)^2 + 0.78\log_{10}(\varepsilon) + 1.20, & \log_{10}(\varepsilon) \geq -2.1 \\ 0.2, & \log_{10}(\varepsilon) < -2.1 \end{cases}$	0.94
20	$f = \begin{cases} 0.14\log_{10}(\varepsilon)^2 + 0.71\log_{10}(\varepsilon) + 1.11, & \log_{10}(\varepsilon) \geq -2.0 \\ 0.24, & \log_{10}(\varepsilon) < -2.0 \end{cases}$	0.95

Table 2. Relationships between the crack density and f-parameter for fixed spherical porosity values for the case of gas-saturated voids. The R^2 is the coefficient of determination.

$\varphi_{\mathbf{pore}}$, %	Equation	$\mathbf{R^2}$
Berryman-SC − Berryman-f and GSA-SC − GSA-f		
2	$f = \begin{cases} 0.04\log_{10}(\varepsilon)^2 + 0.51\log_{10}(\varepsilon) + 1.30, & \log_{10}(\varepsilon) \geq -3.5 \\ 0.15, & \log_{10}(\varepsilon) < -3.5 \end{cases}$	0.94
5	$f = \begin{cases} 0.07\log_{10}(\varepsilon)^2 + 0.56\log_{10}(\varepsilon) + 1.18, & \log_{10}(\varepsilon) \geq -3.0 \\ 0.18, & \log_{10}(\varepsilon) < -3.0 \end{cases}$	0.98
10	$f = \begin{cases} 0.09\log_{10}(\varepsilon)^2 + 0.56\log_{10}(\varepsilon) + 1.10, & \log_{10}(\varepsilon) \geq -3.0 \\ 0.20, & \log_{10}(\varepsilon) < -3.0 \end{cases}$	0.98
15	$f = \begin{cases} 0.10\log_{10}(\varepsilon)^2 + 0.54\log_{10}(\varepsilon) + 1.07, & \log_{10}(\varepsilon) \geq -2.5 \\ 0.30, & \log_{10}(\varepsilon) < -2.5 \end{cases}$	0.97
20	$f = \begin{cases} 0.07\log_{10}(\varepsilon)^2 + 0.42\log_{10}(\varepsilon) + 1.01, & \log_{10}(\varepsilon) \geq -2.0 \\ 0.40, & \log_{10}(\varepsilon) < -2.0 \end{cases}$	0.97
DEM − Berryman-f		
2	$f = \begin{cases} 0.01\log_{10}(\varepsilon)^2 + 0.38\log_{10}(\varepsilon) + 1.14, & \log_{10}(\varepsilon) \geq -3.3 \\ 0.13, & \log_{10}(\varepsilon) < -3.3 \end{cases}$	0.94
5	$f = \begin{cases} -0.03\log_{10}(\varepsilon)^3 - 0.08\log_{10}(\varepsilon)^2 + 0.34\log_{10}(\varepsilon) + 1.10, & \log_{10}(\varepsilon) \geq -3.0 \\ 0.11, & \log_{10}(\varepsilon) < -3.0 \end{cases}$	0.98
10	$f = \begin{cases} 0.09\log_{10}(\varepsilon)^2 + 0.60\log_{10}(\varepsilon) + 1.07, & \log_{10}(\varepsilon) \geq -3.0 \\ 0.14, & \log_{10}(\varepsilon) < -3.0 \end{cases}$	0.98
15	$f = \begin{cases} 0.10\log_{10}(\varepsilon)^2 + 0.57\log_{10}(\varepsilon) + 0.99, & \log_{10}(\varepsilon) \geq -2.5 \\ 0.19, & \log_{10}(\varepsilon) < -2.5 \end{cases}$	0.98
20	$f = \begin{cases} 0.10\log_{10}(\varepsilon)^2 + 0.53\log_{10}(\varepsilon) + 0.94, & \log_{10}(\varepsilon) \geq -2.0 \\ 0.23, & \log_{10}(\varepsilon) < -2.0 \end{cases}$	0.97

4. Discussion

We analyze several methods of rock physics that give a possibility of taking into account the effect of pore space connectivity in carbonate rock. Some of these methods,

namely, GSA-SC, Berryman-SC, and DEM, allow us to do that implicitly. Thus, the derivation schemes of formulas for GSA-SC and Berryman-SC methods assume that each inclusion of ellipsoidal shape is placed in a matrix with effective properties thereby implicitly allowing the inclusions to be in a contact with each other. The DEM method, at each step, requires placing a portion of inclusions in a medium that already contains several portions of inclusions embedded in the previous steps. The elastic properties of this medium change after each step. This means that the inclusions of every new step can be in a contact with previously embedded inclusions.

The other two methods considered in our work, GSA-*f* and Berryman-*f*, can quantify the effect of pore space connectivity via a special dimensionless parameter f varying from 0 to 1. This parameter controls the properties in so-called comparison body in Formulas (3), (5), (8), and (9), being a coefficient in the linear combination of stiffness tensors of the stiffest and softest materials composing a rock. The comparison body serves as a host medium for other inclusions. The case $f = 0$ is related to a matrix having properties of the stiffest component with isolated ellipsoidal inclusions of other components. The opposite limiting case $f = 1$ is related to the medium where the softest component plays the role of the host matrix. In the case of porous rock, the first case corresponds to completely isolated inclusions in a mineral matrix. The second limiting case comprises an exotic medium with a fluid matrix with ellipsoidal solid particles of mineral matter, kerogen, etc. The f values between 0 and 1 are related to intermediate cases met in reality. The increase in this parameter means that the voids become more connected and vice versa. This parameter is non-measurable and can be evaluated by inversion from experimental data with the use of rock-physics modeling [36,43].

To clarify the physical meaning of the f-parameter, we compare two simple rock-physics models of carbonate rock. Porous-cracked limestone is considered. The first model (Type 1 model) is a double porosity model representing isotropic calcite polycrystal with two types of voids: spherical pores and randomly oriented cracks having various aspect ratios. To calculate the effective elastic properties of this model we apply two methods based on the self-consistent approach of the effective medium theory including GSA-SC, Berryman-SC, and DEM. The second model (Type 2 model) is the same isotropic calcite polycrystal with spherical pores whose connectivity is described by the f-parameter according to formulas of GSA-*f* and Berryman-*f* methods (Equations (1)–(5) and (6)–(9), respectively).

Our idealized models (Figure 1) reflect specific microstructure that could be met for isotropic carbonates in practice [43,52–54]. These idealized models are often used to estimate the effective elastic properties of reservoir rocks. Specifically, these are simplest models for porous-fractured carbonate reservoir rocks that are of vital interest for prospecting geophysics. These idealized models have predictive power and help to assess the elastic wave velocities change if: (1) the crack porosity increases (or decreases), (2) the crack relative opening increases (decreases), (3) crack density increases (decreases), (4) the fluid type varies and so on. Specifically, these models are applied for well-log and seismic data in order to localize and characterize the fractured zones [55,56].

To analyze how the f-parameter is related to characteristics of pore/crack space, we calculate the effective elastic moduli of carbonate rock using the five mentioned above methods varying the model parameters in a wide range. Then, among the obtained solutions for the effective bulk and shear moduli, we choose those that could be called "similar" and associate the f-parameter provided by a Type 2 model with the respective crack characteristics provided by a selected Type 1 model. We analyze three pairs of models (Type 1 model − Type 2 model): (1) GSA-SC − GSA-*f*, (2) Berryman-SC − Berryman-*f*, and (3) DEM − Berryman-*f*.

The results of our analysis demonstrate that the f-parameter can be associated with cracks in a double porosity model. Thus, an increase in the crack porosity (Figures 2 and 3) or crack density (Figure 4) is accompanied by an increase in the f-parameter values. For cracks of aspect ratio 10^{-3} and higher, if we keep the crack porosity constant but increase the spherical porosity the f-parameter becomes to decrease. This is explained by diminishing

the crack contribution to the overall effect of porosity on the elastic moduli. This result is consistent with the findings of [34] showing that the f-parameter is proportional to the logarithm of the ratio of permeability to porosity. It is interesting that this effect is not observed for very thin (aspect ratio around 10^{-4}) gas-saturated cracks. In this case, high values of the f-parameter are seen in the whole range of spherical porosity. These results suggest that f-models have a good chance to detect and quantify the zones of enhanced fracturing and hence permeability.

Note that a good correlation between the f-parameter with crack density gives favor to f-models in characterizing the fractured zones. The f-models (Type 2 models) contain only one parameter in contrast to Type 1 models which incorporate two parameters to specify cracks. Commonly, a wide range of combinations (crack porosity, crack aspect ratio) could be inverted from measured elastic wave velocities and density, based on the rock-physics modeling. These characteristics of cracks are very difficult to estimate experimentally in order to impose bounds on the possible solutions. The use of crack density allows one to decrease the non-uniqueness in the characterization of fractured zones. Note that Hudson's [57,58] model for effective elastic properties of rock with aligned cracks also operates with a single parameter characterizing cracks, namely, crack density instead of the pair "crack aspect ratio, crack porosity". Besides, the inversion based on the f-models works faster compared to the inversion based on the self-consistent models due to the smaller number of unknowns and absence of iterations. This fact is significant in the case when the inversion should be performed for a large number of wells with extended depth intervals of interest.

The theoretical models should be validated, ideally, on artificial samples with known geometry of inclusions. Such a validation of f-model was carried out in [29]. However, in the case of rocks, this type of validation is quite complex and may be possible with the use of digital rock approach based on data of electron microscopy or computed tomography. Besides, the parameter f in the second model has no an experimentally measurable analog. In addition, along this way, other problems arise. For example, so-called segmentation problem exists that gives a solution to the question of where the solid material ends and the void begins. This problem is not easily solved for carbonate samples due to their specific microstructure. Another problem in the digital rock approach is that the properties of intergranular material should be incorporated in the digital model but they are difficult to determine.

We have a few examples of "indirect" validating of the effective medium models. The authors [31] applied the GSA method for the effective permeability modeling for Barnett shale. They showed that, for this modeling, the permeability of fluid-saturated zones should be also specified (or inverted from the permeability measurements). Besides, it was demonstrated that the f-parameter inverted from measured permeability has values similar to that inverted from the elastic wave velocities. In another work authors using the modified GSA method with f-parameter demonstrated prediction of the hydraulic permeability and thermal conductivity of clastic rocks from logging data on Vp and electrical conductivity [32]. The predicted permeability is in good agreement with the measured on full-size core samples.

The question of the model simplicity is debatable. According to Dvorkin [59], a rock-physics model should be "as simple as possible but not simpler". The meaning of this phrase is that the model simplicity is dictated by availability of experimental data and the goal of modeling. Definitely, in a real rock, the pores and cracks exhibit a variety of shapes and sizes. At the core scale we have many tools to examine the rock microstructure (optical and electron microscopy, CT scanning, direct observation of samples). In this case, a rock-physics model can incorporate different type of voids. An example is a very popular the Xu-Payne model [60] of carbonate rocks that includes four types of voids: micropores, clay-related non-isometric voids, cracks, and macropores. Each type of void is described by its specific aspect ratio. This model contains seven parameters of microstructure describing the shape and volume concentration of voids of different types.

Another example is the Xu-White model of clayey sandstones containing silt-related and clay-related pores of different aspect ratios [61]. This model contains three microstructural parameters—aspect ratios of silt- and clay-related voids and a parameter describing the porosity distribution between the silt and clayey parts. Commonly, the microstructural parameters are inverted from two elastic wave velocities (Vp and Vs) measured on rock samples or provided by logs. The number of unknowns in these models is greater than the number of measurements which leads to a wide domain of possible solutions. However, constrains provided by microstructural analysis narrow this domain. If the inversion is not supported by microstructural analysis in such complex models the found model parameters have no sense and only play a role in fitting parameters. In this case, simpler models should be applied. However, a model should not be oversimplified. Thus, sometimes the effective elastic properties of carbonate rocks are based on a model consisting of carbonate matrix with a single type of inclusions [62–65]. A disadvantage of oversimplified models is that they may provide an erroneous prediction. Thus, in the work [66] it is shown that a model with a single aspect ratio used for all voids and a model that distinguishes between the pores and cracks produce different predictions for elastic wave velocities if the fluid type changes. In both models the self-consistent scheme of EMT was applied.

If a rock exhibits a hierarchical structure at the scale of consideration and contains several groups of heterogeneities having different sizes, the rock physics model is constructed according to the rule "from smaller to larger heterogeneities", and the modeling assumes different stages (like in the Xu–Payne model). At stages when it is necessary to insert connected voids, the f-models can be applied, which leads to a decrease in the number of model parameters. Note that the replacement of crack characteristics by the f-parameter is applicable for any matrix, not only for calcite polycrystal.

Moreover, we can speak about two approaches to model design: conceptual models and data-driven models. The first one addresses the fit-for-purpose mind set [67] and represents the essential and reasonable features of the detailed geological structure of the rocks. This is in line with Dvorkin's [59] approach to modeling. The second one tends to make the models as complex as the geology is believed to be. The tools such as electron microscopy and CT scanning provide us the evidence that the rocks are considerably more complex in detail than we are capable of modelling explicitly. Yet the data-driven models rely on the statistical content of the investigating data set and in the reality this data set is usually statistically insufficient. Separately, from a practical point of view, much of these details are irrelevant to further reservoir modeling and hence for economic or engineering decisions [67].

We believe in the compromising approach which relies on building a detailed model as available experimental data enables us and then according to the modeling purpose provide the sensitivity study to simplify the model.

5. Conclusions

Methods of effective medium theory give a possibility of taking into account the void's connectivity. Some of the methods allow to do this implicitly (self-consistent methods of Berryman and GSA, differential scheme), and the other methods include a special parameter quantifying the connectivity (f-models of GSA and Berryman-like approach). A comparison of results obtained with two groups of EMT methods allows us to conclude that the parameter f is controlled by the portion of fractures in the total pore volume, and an increase in the crack porosity is accompanied by increase in the f-parameter. A valuable correlation of the crack density ε and f-parameter is established which, in general, has the form $f = a \log_{10}(\varepsilon)^2 + b \log_{10}(\varepsilon) + c$ for $\varepsilon \leq \varepsilon_{min}$. For the crack density less than ε_{min} the f-parameter can be approximated by a constant value f_{min}. The values of ε_{min} and f_{min} and coefficients a, b, and c depend on the porosity of spherical pores, saturation type, and pair of methods used for finding the link. This allows us to conclude that enhanced values of the f-parameter inverted from experimental data on elastic wave velocities can help to localize zones of enhanced fracturing and, thereby, the enhanced permeability.

The obtained results give a favor for f-models to localize fractured zones from well-log data since they have only a single parameter specifying fractures. The inversion based on models with fewer unknown parameters is more stable and produces a narrow domain of possible solutions. In addition, the inversion works faster compared to the case of a larger number of unknowns.

The use of methods based on f-parameter instead of SCA-based methods can also reduce the total number of parameters in complex rock-physics models. This is the case when a model requires input of pores and cracks at certain stage(s) but estimation of their characteristics (e.g., relative opening) based on microstructural analysis meets difficulties.

Author Contributions: Conceptualization, I.B. (Irina Berezina) and I.B. (Irina Bayuk); methodology, I.B. (Irina Berezina); software, I.B. (Irina Berezina); validation, I.B. (Irina Berezina) and I.B. (Irina Bayuk); formal analysis, I.B. (Irina Berezina) and I.B. (Irina Bayuk); investigation, I.B. (Irina Berezina) and I.B. (Irina Bayuk); resources, I.B. (Irina Berezina) and I.B. (Irina Bayuk); data curation, I.B. (Irina Berezina); writing—original draft preparation, I.B. (Irina Berezina); writing—review and editing, I.B. (Irina Berezina) and I.B. (Irina Bayuk); visualization, I.B. (Irina Berezina); supervision, I.B. (Irina Bayuk); project administration, I.B. (Irina Berezina) and I.B. (Irina Bayuk); funding acquisition, I.B. and I.B. (Irina Bayuk). All authors have read and agreed to the published version of the manuscript.

Funding: This research was performed as part of the State assignment of Schmidt Institute of Physics of the Earth RAS.

Institutional Review Board Statement: Not relevant to this study.

Informed Consent Statement: Not applicable.

Data Availability Statement: All simulation results can be found via this link https://cloud.mail.ru/public/gEWJ/gtAKUnvGA (accessed on 7 September 2022).

Conflicts of Interest: The authors declare no conflict of interest.

References

1. Carman, P.C. Fluid flow through granular beds. *Trans. Inst. Chem. Eng.* **1937**, *15*, 150. [CrossRef]
2. Dullien, F.A.L. *Porous Media: Fluid Transport and Pore Structure*; Academic Press: San Diego, CA, USA, 1979.
3. Adler, P.M. *Porous Media: Geometry and Transport*; Butterworth-Heinemann: Boston, MA, USA, 1992.
4. Gueguen, Y.; Palciauskas, V. *Introduction to the Physics of Rocks*; Princeton University Press: Princeton, NJ, USA, 1994.
5. Sahimi, M. *Flow and Transport in Porous Media and Fractured Rock*; VCH: Weinheim, Germany, 1995.
6. Tondi, E.; Rustichelli, A.; Cilona Balsamo, F.; Storti, F.; Napoli, G.; Napoli, G.; Renda, P.; Giorgioni, M. Hydraulic properties of fault zones in porous carbonates, examples from central and southern Italy. *Italian J. Geosci.* **2016**, *135*, 68–79. [CrossRef]
7. Qian, C.; Li, X.; Shen, W.; Zhang, Q.; Guo, W.; Hu, Y.; Cui, Y.; Jia, Y. Study on the Pore Structure and Fractal Characteristics of Different Lithofacies of Wufeng–Longmaxi Formation Shale in Southern Sichuan Basin, China. *ACS Omega* **2022**, *7*, 8724–8738. [CrossRef] [PubMed]
8. Li, J.; Li, X.-R.; Song, M.-S.; Liu, H.-M.; Feng, Y.-C.; Liu, C. Investigating microscopic seepage characteristics and fracture effectiveness of tight sandstones: A digital core approach. *Petrol. Sci.* **2021**, *18*, 173–182. [CrossRef]
9. Yang, Y.-F.; Wang, K.; Lv, Q.-F.; Askari, R.; Mei, Q.-Y.; Yao, J.; Hou, J.-X.; Zhang, K.; Li, A.-F.; Wang, C.-C. Flow simulation considering adsorption boundary layer based on digital rock and finite element method. *Petrol. Sci.* **2021**, *18*, 183–194. [CrossRef]
10. Jia, B.; Xian, C.-G. Permeability measurement of the fracture-matrix system with 3D embedded discrete fracture model. *Petrol. Sci.* **2022**, *19*, 1757–1765. [CrossRef]
11. Arzilli, F.; Cilona, A.; Mancini, L.; Tondi, E. Using synchrotron X-ray microtomography to characterize the pore network of reservoir rocks: A case study on carbonates. *Adv. Water Resour.* **2016**, *95*, 254–263. [CrossRef]
12. Zambrano, M.; Tondi, E.; Mancini, L.; Arzilli, F.; Lanzafame, G.; Materazzi, M.; Torrieri, S. 3D Pore-network quantitative analysis in deformed carbonate grainstones. *Mar. Pet. Geol.* **2017**, *82*, 251–264. [CrossRef]
13. Koestel, J.; Larsbo, M.; Jarvis, N. Scale and REV analyses for porosity and pore connectivity measures in undisturbed soil. *Geoderma* **2020**, *366*, 114206. [CrossRef]
14. Bernabé, Y.; Li, M.; Maineult, A. Permeability and pore connectivity: A new model based on network simulations. *J. Geophys. Res.* **2010**, *115*, B10203. [CrossRef]
15. Bernabé, Y.; Zamora, M.; Li, M.; Maineult, A.; Tang, Y.B. Pore connectivity, permeability and electrical formation factor: A new model and comparison to experimental data. *J. Geophys. Res.* **2011**, *116*, B11204. [CrossRef]
16. Bernabé, Y.; Maineult, A. *Physics of porous media: Fluid flow through porous media. Treatise on Geophysics*, 2nd ed.; Schubert, G., Ed.; Elsevier Science and Technology: Oxford, UK, 2015; Volume 11, pp. 19–41.

17. Lucas, M.; Vetterlein, D.; Vogel, H.-J.; Schlüter, S. Revealing pore connectivity across scales and resolutions with X-ray CT. *Eur. J. Soil Sci.* **2021**, *72*, 546–560. [CrossRef]
18. Biswal, B.; Manwart, C.; Hilfer, R. Three-dimensional local porosity analysis of porous media. *Phys. A Stat. Mech. Its Appl.* **1998**, *255*, 221–241. [CrossRef]
19. Keller, L.M.; Holzer, L.; Schuetz, P.; Gasser, P. Pore space relevant for gas permeability in Opalinus clay: Statistical analysis of homogeneity, percolation, and representative volume element. *J. Geophys. Res. Solid Earth* **2013**, *118*, 2799–2812. [CrossRef]
20. Mu, Y.; Sungkorn, R.; Toelke, J. Identifying the representative flow unit for capillary dominated two-phase flow in porous media using morphology-based porescale modeling. *Adv. Water Resour.* **2016**, *95*, 16–28. [CrossRef]
21. Bruns, S.; Stipp, S.L.S.; Sorensen, H.O. Statistical representative elementary volumes of porous media determined using greyscale analysis of 3D tomograms. *Adv. Water Resour.* **2017**, *107*, 32–42. [CrossRef]
22. Glover, P.W.J. What is the cementation exponent? A new interpretation. *Lead. Edge* **2009**, *28*, 82–85. [CrossRef]
23. Montaron, B. Connectivity Theory—A new approach to modeling non-Archie rocks. *Petrophysics* **2009**, *50*, 102–115.
24. Kirkpatrick, S. Percolation and Conduction. *Rev. Mod. Phys.* **1973**, *45*, 574–588. [CrossRef]
25. Trinchero, P.; Sánchez-Vila, X.; Fernàndez-Garcia, D. Point to-point connectivity, an abstract concept or a key issue for risk assessment studies? *Adv. Water Resour.* **2008**, *31*, 1742–1753. [CrossRef]
26. Bruggeman, D.A.G. Berechnung verschiedener physikalischer Konstanten von heterogenen Substanzen. *Ann. Phys.* **1935**, *24*, 636–679. [CrossRef]
27. Kirkpatrick, S. Classical transport in disordered media: Scaling and effective-medium theories. *Phys. Rev. Lett.* **1971**, *27*, 1722–1725. [CrossRef]
28. Shermergor, T.D. *Theory of Elasticity of Heterogeneous Media*; Nauka: Moscow, Russia, 1977. (In Russian)
29. Bayuk, I.O.; Chesnokov, E.M. Correlation between elastic and transport properties of porous cracked anisotropic media. *Phys. Chem. Earth* **1998**, *23*, 361–366. [CrossRef]
30. Jakobsen, M. Effective hydraulic properties of fractured reservoirs and composite porous media. *J. Seism. Explor.* **2007**, *16*, 199–224.
31. Chesnokov, E.; Bayuk, I.; Metwally, Y. Inversion of shale microstructure parameters from permeability measurements. In *SEG Technical Program Expanded Abstracts 2010*; Society of Exploration Geophysicists: Houston, TX, USA, 2010; pp. 2634–2638.
32. Bayuk, I.; Goloshubin, G.; Tcimbaluk, Y.; Borkun, F. Rock-Physics based prediction of hydraulic permeability and thermal conductivity of anisotropic clastic rocks from logging data. In *SEG Technical Program Expanded Abstracts 2016*; Society of Exploration Geophysicists: Dallas, TX, USA, 2016; pp. 3155–3158.
33. Eshelby, J.D. The determination of the elastic field of an ellipsoidal inclusions and related problems. *Proc. R. Soc. Lond. Ser. A Math. Phys. Sci.* **1957**, *241*, 376–396.
34. Berryman, J.G. Long-wavelength propagation in composite elastic media. *J. Acoust. Soc. Am.* **1980**, *68*, 1809–1831. [CrossRef]
35. Berryman, J.G.; Pride, S.R.; Wang, H.F. A differential scheme for elastic properties of rocks with dry or saturated cracks. In Proceedings of the 15th ASCE Engineering Mechanics Conference, New York, NY, USA, 2–5 June 2002.
36. Bayuk, I.O.; Ammerman, M.; Chesnokov, E.M. Elastic moduli of anisotropic clay. *Geophysics* **2007**, *72*, D107–D117. [CrossRef]
37. Willis, J. Bounds and self-consistent estimates for the overall properties of anisotropic composites. *J. Mech. Phys. Solids* **1977**, *25*, 185–202. [CrossRef]
38. Jiang, T. Connection of Elastic and Transport Properties: Effective Medium Study in Anisotropic Porous Media. Ph.D. Thesis, Faculty of the Department of Earth and Atmospheric Sciences University of Houston, Houston, TX, USA, 2013.
39. Biot, M.A. General theory of three-dimensional consolidation. *J. Appl. Phys.* **1941**, *12*, 155–164. [CrossRef]
40. Biot, M.A.; Willis, D.G. The elastic coefficients of theory of consolidation. *J. Appl. Mech.* **1957**, *24*, 594–601. [CrossRef]
41. Chesnokov, E.M.; Ammerman, M.; Sinha, S.; Kukharenko, Y.A. Tensor character of Biot parameter in poroelastic anisotropic media under stress: Static and dynamic cases. In Proceedings of the Rainbow in the Earth-2nd International Workshop, Berkeley, CA, USA, 17–18 August 2005.
42. Terzaghi, K. Van Die Berechnung der Durchassigkeitsziffer des Tones aus dem Veriauf der hydrodynamischen Spannungserscheinungen. *Sitzungsber. Akad. Wiss. Wien Math Naturwiss.* **1923**, *132*, 105.
43. Ghasemi, M.; Bayuk, I. Application of rock physics modelling to investigate the differences between static and dynamic elastic moduli of carbonates. *Geophys. J. Int.* **2020**, *222*, 1992–2023. [CrossRef]
44. Budiansky, B. On the elastic moduli of some heterogeneous materials. *J. Mech. Phys. Solids* **1965**, *13*, 223–227. [CrossRef]
45. Hill, R. A self-consistent mechanics of composite materials. *J. Mech. Phys. Solids* **1965**, *13*, 213–222. [CrossRef]
46. Wu, T.T. The effect of inclusion shape on the elastic moduli of a two-phase material. *Int. J. Solids Struct.* **1966**, *2*, 1–8. [CrossRef]
47. Christensen, R.M.; Lo, K.H. Solutions for effective shear properties in three phase sphere and cylinder models. *J. Mech. Phys. Solids* **1979**, *27*, 315–330. [CrossRef]
48. Kuster, G.T.; Toksoz, M.N. Velocity and attenuation of seismic waves in two-phase media. *Geophysics* **1974**, *39*, 587–618. [CrossRef]
49. Nishizawa, O. Seismic velocity anisotropy in a medium containing oriented cracks—Transversely isotropic case. *J. Phys. Earth* **1982**, *30*, 331–347. [CrossRef]
50. Norris, A.N.; Sheng, P.; Callegari, A.J. Effective-medium theories for two-phase dielectric media. *J. Appl. Phys.* **1985**, *57*, 1990–1996. [CrossRef]
51. Jakobsen, M.; Hudson, J.A.; Minshull, T.A.; Singh, S.C. Elastic properties of hydrate-bearing sediments using effective medium theory. *J. Geoph. Res.* **2000**, *105*, 561–577. [CrossRef]

52. Newberry, B.M.; Grace, L.M.; Stief, D.O. Analysis of Carbonate Dual Porosity Systems from Borehole Electrical Images. In Proceedings of the Permian Basin Oil & Gas Recovery Conference, Midland, TX, USA, 27–29 March 1996.
53. Kazatchenko, E.; Markov, M.; Mousatov, A. Joint Inversion of Acoustic and Resistivity Data for Carbonate Microstructure Evaluation. *Petrophysics* **2004**, *45*, 130–140.
54. Sun, J.; Chi, P.; Cheng, Z.; Yang, L.; Yan, W.; Cui, L. A novel saturation calculation model of fractured-vuggy carbonate reservoir via multiscale pore networks: A case study from Sichuan Basin, China. *J. Geophys. Eng.* **2021**, *18*, 85–97. [CrossRef]
55. Dubinya, N.; Bayuk, I.; Tikhotskiy, S.; Rusina, O. Localization and characterization of hydraulically conductive fractured zones at seismic scale with the help of Geomecha. In Proceedings of the 80th EAGE Conference and Exhibition, Copenhagen, Denmark, 11–14 June 2018.
56. Bayuk, I.O.; Dubinya, N.V.; Garagash, I.A.; Tikhotskiy, S.A.; Tikhotskaya, O.A. Multiscale Rock-physics modeling of effective elastic properties of fractured reservoir rocks. In Proceedings of the 53rd US Rock Mechanics/Geomechanics Symposium, ARMA, New York, NY, USA, 23–26 June 2019; pp. 19–415.
57. Hudson, J.A. Overall properties of a cracked solid. *Math. Proc. Camb. Phil. Soc.* **1980**, *88*, 371–384. [CrossRef]
58. Hudson, J.A. Wave speeds and attenuation of elastic waves in material containing cracks. *Geophys. J. R. Astron. Soc.* **1981**, *64*, 133–150. [CrossRef]
59. Dvorkin, J. Honorary Lecture "Modern Rock Physics—Challenges and Solutions". Seismic Soundoff. In-Depth Conversations in Applied Geophysics 2021, Episode 126. Available online: https://seg.org/podcast/post/13574 (accessed on 1 September 2022).
60. Xu, S.; Payne, M.A. Modeling elastic properties in carbonate rocks. *Lead. Edge* **2009**, *28*, 66–74. [CrossRef]
61. Xu, S.; White, R.E. A new velocity model for clay-sand mixtures. *Geophys. Prosp.* **1995**, *43*, 91–118. [CrossRef]
62. Fournier, F.; Léonide, P.; Kleipool, L.; Toullec, R.; Reijmer, J.J.G.; Borgomano, J.; Klootwijk, T.; Van Der Molen, J. Pore space evolution and elastic properties of platform carbonates (Urgonian limestone, Barremian-Aptian, SE France). *Sediment. Geol.* **2014**, *308*, 1–17. [CrossRef]
63. Fournier, F.; Pellerin, M.; Villeneuve, Q.; Teillet, T.; Hong, F.; Poli, E.; Borgomano, J.; Philippe, L.; Hairabian, A. The equivalent pore aspect ratio as a tool for pore type prediction in carbonate reservoirs. *AAPG Bulletin* **2018**, *102*, 1343–1377. [CrossRef]
64. Guo, Z.; Qin, X.; Zhang, Y.; Niu, C.; Wang, D.; Ling, Y. Numerical investigation of the effect of heterogeneous pore structures on elastic properties of tight gas sandstones. *Front. Earth Sci.* **2021**, *9*, 641637. [CrossRef]
65. Markov, M.; Kazatchenko, E.; Mousatov, A. Compressional and shear wave velocities in multicomponent carbonate media as porosity functions. In Proceedings of the SPWLA 47th Annual Logging Symposium, Veracruz, Mexico, 4–7 June 2006.
66. Bayuk, I. Role of internal structure of rocks in the construction of their petroelastic models. *Geofizika* **2022**, *3*, 2–8. (In Russian)
67. Ringrose, P.; Bentley, M. Reservoir Model Design. In *A Practitioner's Guide*; Springer: Berlin/Heidelberg, Germany; New York, NY, USA; London, UK, 2015. [CrossRef]